Applied Catalysis B: Environmental 174–175 (2015) 421–426

Contents lists available at ScienceDirect

Applied Catalysis B: Environmental

journal homepage: www.elsevier.com/locate/apcatb

TiO_2/RGO composite aerogels with controllable and continuously tunable surface wettability for varied aqueous photocatalysis

Wenjun Liu, Jingyu Cai, Zhengxin Ding*, Zhaohui Li**

Research Institute of Photocatalysis, State Key Laboratory of Photocatalysis on Energy and Environment, College of Chemistry, Fuzhou University, Fuzhou 350002, PR China

ARTICLE INFO

Article history:
Received 10 January 2015
Received in revised form 21 March 2015
Accepted 22 March 2015
Available online 24 March 2015

Keywords:
RGO aerogel
TiO_2
Surface wettability
Photocatalysis
Recycling

ABSTRACT

TiO_2/RGO composite aerogels with TiO_2 nanostructures grown on interconnected three-dimensional RGO porous networks were fabricated via a facile one-pot hydrothermal method. The as-obtained composite aerogels show controllable and continuously tunable surface wettability from super-hydrophobic to super-hydrophilic depending on the amount of incorporated TiO_2. The TiO_2/RGO composite aerogels with varied surface wettability can selectively degrade different pollutants in aqueous systems. The capability of forming the TiO_2/RGO aerogels with tunable surface wettability for selective photocatalysis is important since such materials are especially useful in some systems which contain extremely poisonous contaminants in low concentration together with large quantity of un-poisonous chemicals.

1. Introduction

Semiconductor photocatalysis has been widely used in the treatments of all kinds of contaminants [1,2]. Among all the investigated photocatalysts, TiO_2 has attracted extremely attentions since it is nontoxic, cheap and has long term chemical stability [3,4]. However, TiO_2 is typically hydrophilic with a high surface density of hydroxyl groups, which restricts its performance for the photocatalytic degradation of the lipophilic pollutants in aqueous systems since a prerequisite for superior activity of a photocatalyst is its adsorption toward the pollutants [5]. To meet different requirements in aqueous photocatalysis, it is therefore desirable to develop TiO_2 with tunable surface wettability.

Generally hydrophobic TiO_2 surface can be obtained by treating TiO_2 nanoparticles with hydrophobic agents like fluorosilane, fatty acid or other hydrophobic reagents [6–8]. However, its performance is inevitably reduced or even eliminated due to the chemical surface modifications. Moreover, the organic agents on the surface are usually costly, poisonous and easily photo-degraded by TiO_2 under UV irradiation, which make the photocatalyst lack the long term stability [9]. An alternative method is to deposit TiO_2 nanoparticles on a hydrophobic support. Functionalized hydrophobic zeolites, siliceous mesoporous cellular foam, polypropylene membrane and other supports have already been used as supports for TiO_2 nanoparticles to enhance their adsorption toward lipophilic pollutants [10–13]. Among various supports investigated, RGO-based aerogel attracts extensive attentions due to its large specific surface area, open pores for fast mass transportation as well as large amount of surface sites for anchoring the catalysts [14–17]. Its extremely light weight enables it to float on the surface of the reaction system, which allows it to absorb more solar irradiations. Moreover, the RGO building blocks can promote the separation of the photo-generated electrons and holes, which is beneficial to the photocatalysis [18–21]. All these peculiar properties of RGO aerogel, together with our recent discovery that the surface wettability of RGO-based aerogel can be facilely tuned by using different cross-linker, make it especially appealing as support for semiconductor photocatalysts [22]. However, the assembly of semiconductors/RGO composite aerogels with controllable surface wettability for aqueous photocatalysis has never been previously reported.

In this manuscript, we demonstrated a facile one-pot hydrothermal method to fabricate of TiO_2/RGO composite aerogels with controllable and continuously tunable surface wettability ranging from super-hydrophobic to super-hydrophilic. The TiO_2/RGO composite aerogels with varied surface wettability can selectively degrade different pollutants in aqueous systems.

* Corresponding author.
** Corresponding author. Tel.: +86 59183779260; fax: +86 59183779260.
E-mail addresses: zxding@fzu.edu.cn (Z. Ding), zhaohuili1969@yahoo.com (Z. Li).

http://dx.doi.org/10.1016/j.apcatb.2015.03.041
0926-3373/

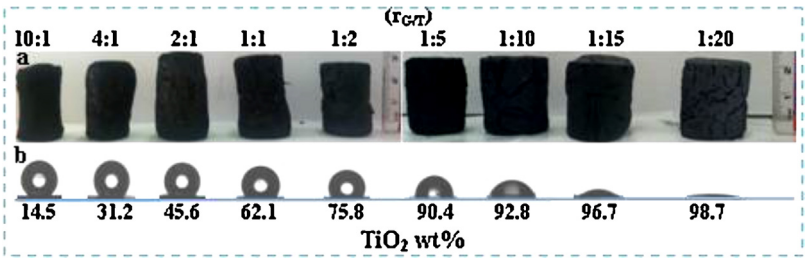

Fig. 1. Photographs of the as-obtained TiO_2/RGO aerogels and the water contact angle of these aerogels with varied weight percentage of TiO_2.

2. Experimental

2.1. Materials

Graphite flake (99.8%, 325 mesh) was provided by Alfa. L-Cysteine (AR) was provided by Aladdin. $TiOSO_4$ (AR) was purchased from Sigma–Aldrich. All the reagents were used without further purification.

2.2. Synthesis of the 3D TiO_2/RGO composite aerogels

Graphene oxide (GO) was synthesized from graphite flake using a modified Hummers method [23]. A certain amount of $TiOSO_4$ was dissolved into 1.4 mg/mL of homogeneous GO aqueous dispersion and 200 mg L-cysteine was added under magnetic stirring. After 30 min, the solution was transferred into a Teflon-sealed autoclave and heated at 160 °C for 10 h. The hydrogels were treated by freeze-drying to obtain TiO_2/RGO aerogels.

2.3. Characterization

The morphology of the product was characterized by a field emission scanning electron microscopy (SEM, JSM-6700F). The transmission electron microscopy (TEM) and high-resolution transmission electron microscopy (HRTEM) images were measured by a JEOL model JEM 2010 EX instrument at an accelerating voltage of 200 kV. Powder X-ray diffraction (XRD) data were collected using a Bruker D8 Advance X-ray diffractometer (Cu-Kα1 irradiation, λ = 1.5406 Å). BET surface area was carried out on an ASAP2020 M apparatus (Micromeritics Instrument Corp., USA). The optical contact angle was characterized by OCA20 optical contact angle device. FT-IR spectra were recorded in transmittance mode with a resolution of 4 cm^{-1} using a Nicolet Nexus 670 FTIR spectrometer. Raman spectroscopy was performed using an invia-Reflex Micro-Raman Spectroscopy system (Renishaw Co.) with 532 nm line of an Ar ion laser at room temperature.

2.4. Photocatalytic activity

The TiO_2/RGO composite aerogel was added into a solution which contains methyl orange (MO, 10 mg/L) and a layer of oleic acid labeled with Sudan III dye. A 300 W Xe lamp with a 360 nm cut-off filter was used as a light source. The TiO_2/RGO composite aerogel floats on the surface of water without stirring during photocatalytic process. At the given time intervals, the analytical sample of MO was taken from the mixture and analyzed by recording variations in the absorption in UV–vis spectra of MO using a Cary 500 ultraviolet visible spectrometer. The process of photo-degradation of oleic acid was monitored by FT-IR spectra of the contaminated aerogel before and after irradiation. The photocatalytic activity of TiO_2/RGO composite aerogels was studied based on TiO_2 mass normalization.

3. Results and discussion

The TiO_2/RGO composite hydrogels were prepared from GO and $TiOSO_4$ hydrothermally using L-cysteine as both cross-linker and reducing agent. Our previous study on the formation of RGO aerogels using cysteine revealed that the optimum condition to obtain the hydrogel is at a weight ratio of GO to cysteine ($r_{G/C}$) of 1:2 [22]. Therefore, the weight ratio of GO to L-cysteine ($r_{G/C}$) was set at 1:2, while the examined weight ratio of GO to $TiOSO_4$ ($r_{G/T}$) ranged from 10:1 to 1:20. Well shaped hydrogels with 3D cylindrical morphology in the macroscopic views, which conform to those of the vessels, can be obtained in the whole examined $r_{G/T}$ ranges. The size of the obtained hydrogels varied a little with different $r_{G/T}$ (Fig. S1). Taking the hydrogel obtained at $r_{G/T}$ of 1:2 as an example, it has a diameter of approximately 20 mm and a height of 35 mm. Upon freeze-drying, the as-obtained hydrogels were dehydrated with monolithic aerogels (Fig. 1a). The XRD patterns of all the obtained samples show diffraction peaks at 2θ of 25.4°, 37.9°, 48.2°, 54,1°, 55.2°, which can be ascribed to (1 0 1), (0 0 4), (2 0 0), (1 0 5) and (2 1 1) crystallographic planes of tetragonal TiO_2 (JCPDF 01-073-1764) (Fig. 2a). At $r_{G/T}$ larger than 4:1, the aerogels also show a diffraction peak at 24.3°, which can be indexed to the (0 0 2) crystal face of RGO. While $r_{G/T}$ lowers than 4:1, as-obtained aerogels do not show any peaks corresponding to GO or RGO [24]. However, even on these aerogels, their FT-IR spectra still show peaks at 1573 cm^{-1}, 1382 cm^{-1} and 1205 cm^{-1} and 1041 cm^{-1}, corresponding to —C=C—, —OH, O—C—O and C—O vibrations. This indicated the successful incorporation of the carbon additive in all the

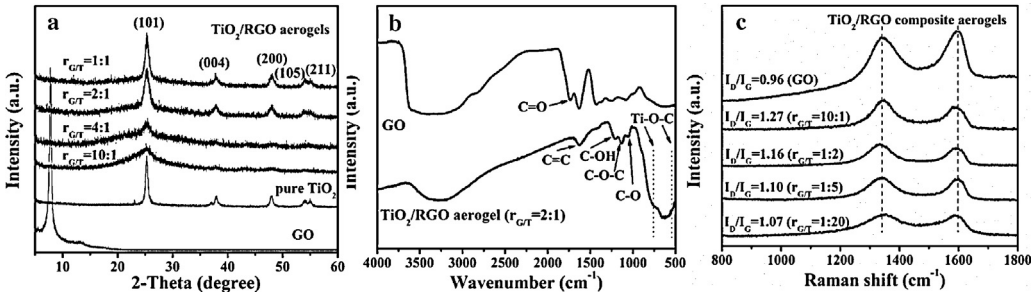

Fig. 2. (a) XRD patterns for pure TiO_2, GO and TiO_2/RGO aerogels (rG/T = 10:1, 4:1, 2:1 and 1:1); (b) FTIR spectra of GO and TiO_2/RGO aerogel at $r_{G/T}$ = 2:1; (c) Raman spectra of GO and TiO_2/RGO aerogels.

Table 1
BET surface area of cys-RGO aerogel, pure TiO_2, TiO_2/RGO aerogels with varied amount of incorporated TiO_2.

			$r_{G/T}$								
	cys-RGO	Pure TiO_2	10:1	4:1	2:1	1:1	1:2	1:5	1:10	1:15	1:20
TiO_2 wt%			14.5	31.2	45.6	62.1	75.8	90.4	92.8	96.7	98.7
S_{BET}[a] (m^2/g)	36	106	232	228	225	201	160	153	146	116	108

[a] Calculated from the linear part of the BET plot (P/P_0 = 0.01–1.0).

composite aerogels. The reduction of GO to RGO during the formation of the aerogels can be evidenced from their FT-IR spectra. As compared to pristine GO, the FT-IR spectra of the as-prepared aerogels show much weaker peaks at 1720 and 3300 cm^{-1}, indicating that most of C=O and —OH on original GO have been reduced (Fig. 2b) [25]. The Raman spectra of all the TiO_2/RGO composite aerogels shows typical D band at ca. 1352 cm^{-1} and G band at ca. 1573 cm^{-1} (Fig. 2c). As compared with GO, the broader D band of all TiO_2/RGO composite aerogels indicates significant structural disorders with the presence of sp^3-hybridised carbons and short-range sp^2-carbon moieties [26]. The intensity ratio of D and G band (I_D/I_G ratio) for TiO_2/RGO composite aerogels ranges from 1.07 for $r_{G/T}$ = 1:20 to 1.27 for $r_{G/T}$ = 10:1, higher than that of original GO (0.96), indicating the introduction of defects during the formation of the TiO_2/RGO aerogel. Moreover, a red-shift of G band from ca. 1593 cm^{-1} for GO to ca. 1573 cm^{-1} for TiO_2/RGO composite aerogels can be assigned to the aggregation of RGO sheets after hydrothermal reaction.

To quantify the amount of TiO_2 incorporated in the TiO_2/RGO composite aerogels, thermo-gravimetric analysis (TGA) was carried out. As shown in Table 1, the weight percentage of TiO_2 in the as-obtained composite aerogels ranged from 14.5% for $r_{G/T}$ = 10:1 to 98.7% for $r_{G/T}$ = 1:20.

All the TiO_2/RGO composite aerogels with TiO_2 weight percentage up to 75.8% consist of interconnected RGO nanosheets to form three-dimensional porous networks, with TiO_2 nanoparticles densely anchored on the RGO surface as evidenced from the SEM image (Fig. 3a). A typical TEM image of TiO_2/RGO composite aerogel (with TiO_2 weight percentage at 75.8%) shows the existence of well dispersed nanoparticles with uniform size of 20–30 nm on the RGO nanosheets (Fig. 3b). The high-resolution TEM (HRTEM) image shows a clear lattice fringe of 0.353 nm, matching that of the (1 0 1) plane of tetragonal TiO_2 (inset in Fig. 3b) [17]. The anchoring of TiO_2 nanoparticles on the RGO nanosheets is expected since it is generally known that the monomeric titanyl ions (TiO^{2+}) can be easily adsorbed on the negative surface of GO owing to the

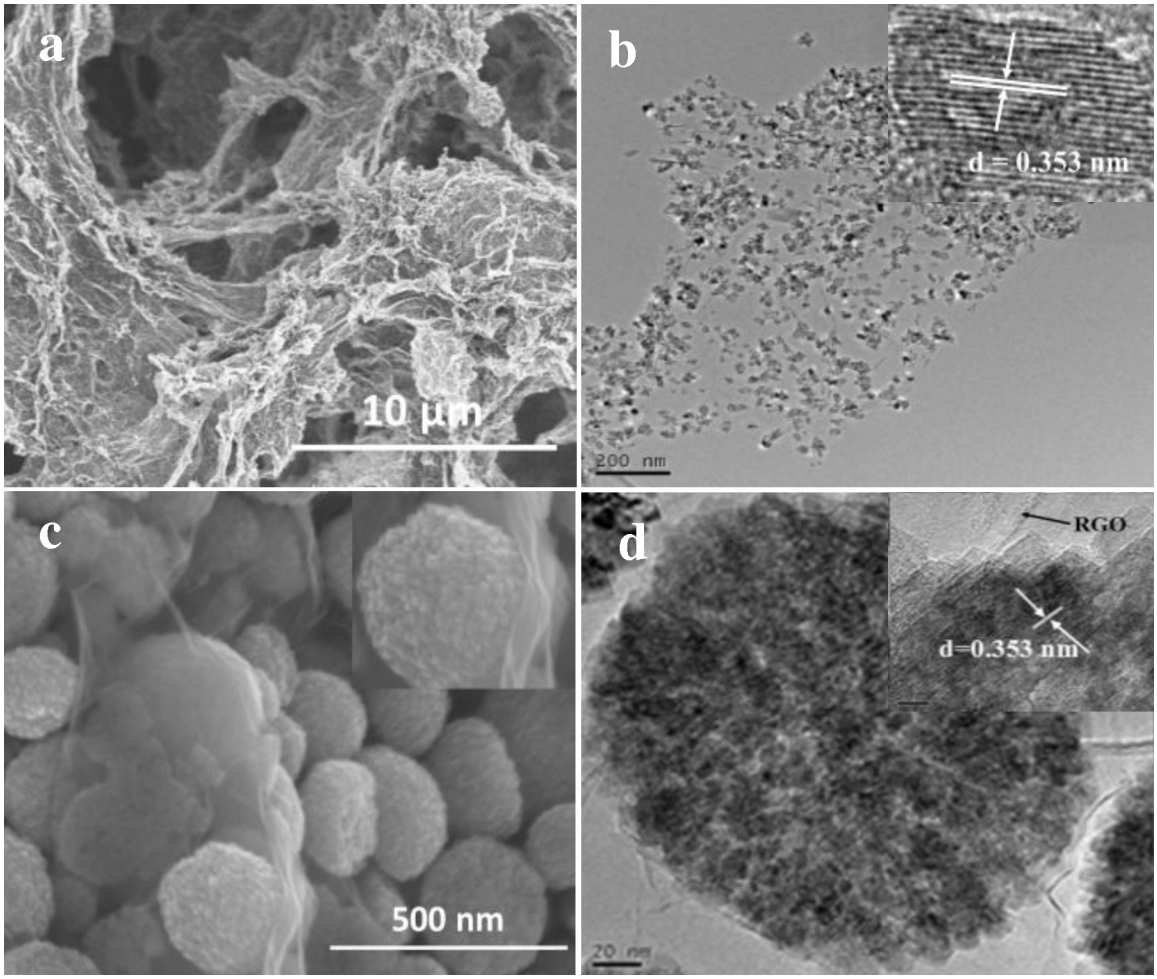

Fig. 3. (a) SEM image and (b) TEM image of TiO_2/RGO aerogel at TiO_2 wt% = 75.8% (inset HRTEM image); (c) SEM image (enlarged SEM image) and (d) TEM image of TiO_2/RGO aerogel at TiO_2 wt% = 96.7% (inset HRTEM image).

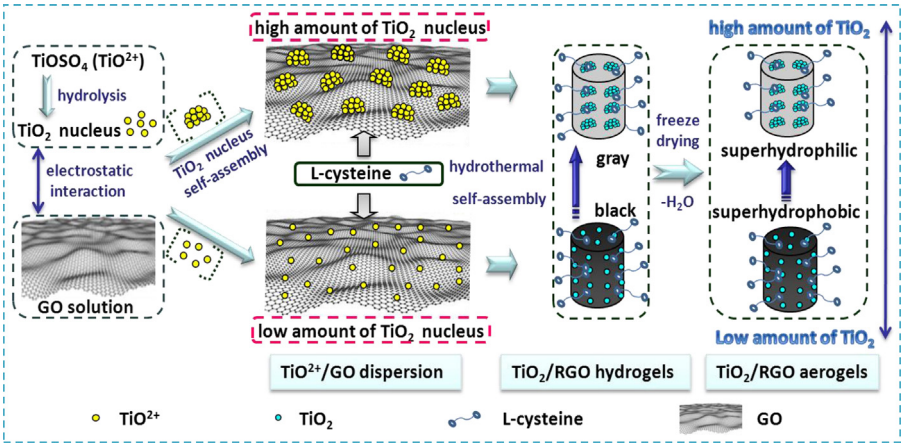

Scheme 1. Schematic illustration of the formations of TiO_2/RGO composite aerogels.

electrostatic interaction [27,28]. The hydrolysis of TiO^{2+} leads to the formation of TiO_2 nuclei on the GO surface [29]. During the hydrothermal treatment, the TiO_2 nuclei grow larger to form the surface anchored TiO_2 nanoparticles, while in the meantime GO is reduced to RGO. The existence of the electrostatic attraction and hydrogen bonds between L-cysteine and RGO together with the π–π stacking between the RGO help to form 3D TiO_2/RGO composite hydrogel. When there is plenty of anchoring sites for the formation of TiO_2 nuclei, the surface anchored TiO_2 nanoparticles do not aggregate and their size is relatively small. That is the case we observed at a lower amount of incorporated TiO_2. However, when the weight percentage of TiO_2 in the TiO_2/RGO composite aerogels is larger than 90.4%, the subsequent self-assembly of TiO_2 nanoparticles around the pre-anchored nuclei particles to form the raspberry-like TiO_2 nano-hemispheres with a mean diameter of approximately 250 nm on ultrathin RGO nanosheets was observed (Fig. 3c) [29–31]. As shown in Fig. 3d, the TEM image of TiO_2/RGO composite aerogel with TiO_2 wt% at 96.7% shows that raspberry-like TiO_2 nano-hemisphere is extremely robust and can sustain prolonged sonication. The formation of the different TiO_2/RGO composite aerogel was illustrated in Scheme 1.

The specific surface area (S_{BET}) of the as-obtained TiO_2/RGO composite aerogels increases with the incorporated RGO and ranges from 108 to 232 m^2/g. The S_{BET} of the TiO_2/RGO aerogels is much larger than either pure RGO-based aerogel (36 m^2/g) or pure TiO_2 (106 m^2/g) prepared similarly (Table 1). This phenomenon is not difficult to understand since TiO_2 nanoparticles in RGO aerogles can act as spacers to prevent the aggregation of the RGO nanosheets, while RGO additive makes TiO_2 dispersed more uniformly [17]. The less aggregation of RGO nanosheets on the composite aerogels as compared with that of pure RGO aerogels can also be evidenced from the SEM images (Fig. 3a and c) [22]. Like pure RGO-based aerogels, all the TiO_2/RGO composite aerogels exhibit high mechanical strength, attributed to the superior mechanical properties of the cross-linked RGO structure. For example, TiO_2/RGO composite aerogel with TiO_2 weight percentage at 75.8% can support a 50 g counterpoise without any deformation of its size and shape (Fig. S2a), while the composite aerogel containing 90.4 wt% of TiO_2 can even bear a 100 g counterpoise (Fig. S2b). This indicates that the incorporation of the inorganic semiconductors onto the RGO aerogel does not reduce the mechanical strength of RGO aerogels.

The as-obtained TiO_2/RGO composite aerogels show varied surface wettability ranging from super-hydrophilic to super-hydrophobic. As shown in Fig. 1b, the contact angle of the as-prepared TiO_2/RGO aerogels varied from 0° (super-hydrophilic) for TiO_2/RGO aerogel with TiO_2 wt% at 96.7% to 157° (super-hydrophobic) for that with TiO_2 wt% at 14.5%. This indicates that the composite aerogels with varied and controllable surface wettability can be facilely obtained via tuning the incorporated amount of TiO_2. The capability to tune the surface wettability of supported TiO_2 photocatalyst is extremely important in view of its practical application for selective degradation of different pollutants in aqueous systems.

To demonstrate the advantage of using the surface wettability tunable TiO_2/RGO composite aerogels for degradation of different organic pollutants in aqueous systems, TiO_2/RGO composite aerogels with different surface wettability were used for the degradation of a aqueous solution containing both lipophilic oleic acid and water-soluble methyl orange (MO). It was found that those aerogels show significantly different photocatalytic performances in this system. The hydrophobic TiO_2/RGO aerogel (with TiO_2 wt% = 75.8%) adsorbs the oleic acid (layered with Sudan III dye) on the surface of the solution very fast. Continuous irradiations on the reaction system can further lead to the degradation of the oleic acid adsorbed on the aerogel as monitored by the FT-IR spectra (Fig. 4a). After 4 h irradiations, the peak at 1712 cm^{-1} which corresponds to C=O vibration of oleic acid significantly weakened, while a complete decomposition of oleic acid can be achieved in 8 h (Fig. 4b). During this period, the degradation of MO can be ignored over the hydrophobic TiO_2/RGO composite aerogel. It is believed that the hydrophobic TiO_2/RGO composite aerogel can keep the hydrophilic molecule away from its surface, which makes it show low activity for MO degradation in aqueous systems. Moreover, all the hydrophobic TiO_2/RGO aerogels show comparable efficiency for the degradation of oleic acid (Fig. S3a). On the contrary, the hydrophilic TiO_2/RGO aerogel (with TiO_2 wt% = 90.4%) only degraded MO and a total degradation occurred in 4 h (Figs. 4c and d and S4). This activity is higher than that over P25 (Fig. S5). A control adsorption experiment revealed that without irradiation, about 49% of MO can be adsorbed on the TiO_2/RGO aerogel (Fig. S6). A high adsorption of the substrate is a prerequisite for its photo-degradation. Similarly, all hydrophilic TiO_2/RGO composite aerogels exhibit excellent photocatalytic performances for decomposition of MO (Fig. S3b) with the highest activity obtained at TiO_2 wt% = 96.7%. Since the photocatalytic activity was studied based on TiO_2 mass normalization, these results indicated that in addition to the amount of TiO_2, other factors may influence the photocatalytic performance of these TiO_2/RGO aerogels. Moreover, both hydrophilic and hydrophobic TiO_2/RGO aerogels (with TiO_2 wt% = 75.8% and 90.4%) show exactly similar performances in either one-component solution or solution containing both MO and oleic acid (Fig. S7). These observations indicate that the as-prepared TiO_2/RGO composite aerogels can show selectivity for the degradation of different contaminants in aqueous systems. The selectivity in photocatalysis is in particular

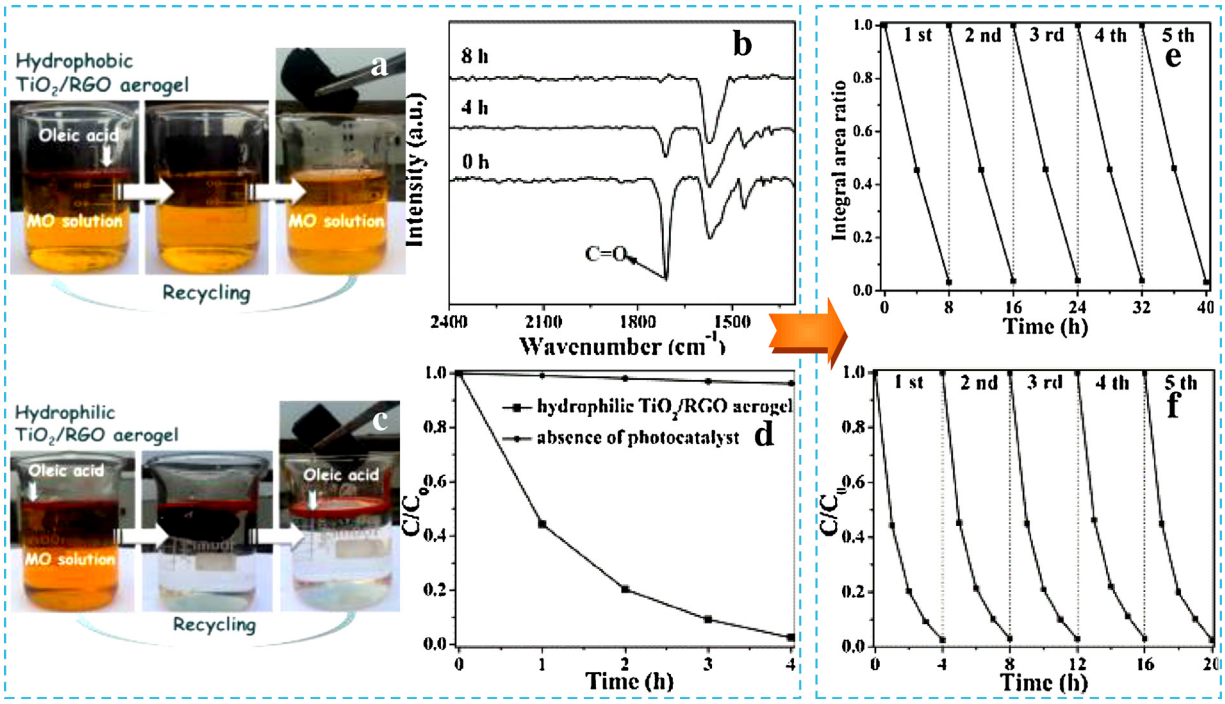

Fig. 4. Photographs which show the adsorption and degradation of mixed contaminants over the as-prepared (a) hydrophobic and (c) hydrophilic TiO_2/RGO aerogels; (b) comparison of the temporal changes of oleic acid concentration as monitored by the FT-IR spectra over the hydrophobic TiO_2/RGO aerogel; (d) comparison of the temporal changes of MO concentration as monitored by the UV–vis absorption spectra at 493 nm over hydrophilic TiO_2/RGO aerogel; cycling runs under irradiation of (e) hydrophobic and (f) hydrophilic TiO_2/RGO aerogels.

useful for some systems that contain extremely poisonous contaminants in low concentration together with a large amount of poisonous chemicals. For comparison, commercial active carbon (AC) supported TiO_2 composites with similar amount of incorporated TiO_2 (with TiO_2 wt% = 75.8% and 90.4%) have also been prepared and their photocatalytic performance has been investigated. It was found that unlike hydrophobic TiO_2/RGO composite aerogel, TiO_2/AC (with TiO_2 wt% = 75.8%) is hydrophilic and sinks at the bottom in aqueous systems, which can not degrade lipophilic oleic acid. Although TiO_2/AC (with TiO_2 wt% = 90.4%) can photodegrade MO, it shows a lower photocatalytic activity than that of hydrophilic TiO_2/RGO composite aerogel with similar amount of incorporated TiO_2 (Fig. S8). This indicates that TiO_2/RGO composite aerogels is superior to other carbon-supported TiO_2 since their surface wettability is tunable and their extremely light weight enables them to float on the surface of the reaction system to adsorb more light. Control experiment showed that the photocatalytic activity of the TiO_2/RGO aerogels is not enhanced when stirred (Fig. S9). No stirring required in the TiO_2/RGO composite aerogels' photocatalysis is extremely appealing for their practical applications. Both hydrophobic and hydrophilic TiO_2/RGO composite aerogels can be easily separated from the reaction systems without loss of any solid photocatalysts and exhibit good recyclability (Fig. 4e and f), which is important for their practical applications.

4. Conclusion

TiO_2/RGO composite aerogels with TiO_2 nanostructures grown on interconnected three-dimensional RGO porous networks have been fabricated by a facile one-pot hydrothermal method. The surface wettability of the as-obtained TiO_2/RGO aerogels varied continuously from super-hydrophilic to super-hydrophobic depending on the amount of incorporated TiO_2. The as-obtained TiO_2/RGO composite aerogels with different surface wettability exhibited selective degradation of different pollutants in aqueous systems. The capability of the formation of TiO_2/RGO aerogels with tunable surface wettability for selective photocatalysis is important since such materials are especially useful in some systems which contain extremely poisonous contaminants in low concentration together with large quantity of unpoisonous chemicals.

Acknowledgments

The work was supported by NSFC (21273035), 973 Program (2014CB239303) and Specialized Research Fund for the Doctoral Program of Higher Education (20123514110002). Z. Li thanks the Award Program for Minjiang Scholar Professorship for financial support.

Appendix A. Supplementary data

Supplementary data associated with this article can be found, in the online version, at http://dx.doi.org/10.1016/j.apcatb.2015.03.041.

References

[1] H. Tong, S.X. Ouyang, Y.P. Bi, N. Umezawa, M. Oshikiri, J.H. Ye, Adv. Mater. 24 (2012) 229–251.
[2] C.C. Chen, W.H. Ma, J.C. Zhao, Chem. Soc. Rev. 39 (2010) 4206–4219.
[3] S.W. Liu, J.G. Yu, M. Jaroniec, Chem. Mater. 23 (2011) 4085–4093.
[4] M. Pelaez, N.T. Nolan, S.C. Pillai, M.K. Seery, P. Falaras, A.G. Kontos, P.S.M. Dunlop, J.W.J. Hamilton, J.A. Byrne, K. O'Shea, M.H. Entezari, D.D. Dionysiou, Appl. Catal. B: Environ. 125 (2012) 331–349.
[5] V. Rico, C. Lopez, A. Borras, J.P. Espinos, A.R. Gonzalez-Elipe, Sol. Energy Mater. Sol. Cells 90 (2006) 2944–2949.
[6] X. Zhang, H. Kono, Z. Liu, S. Nishimoto, D.A. Tryk, T. Murakami, H. Sakai, M. Abeb, A. Fujishima, Chem. Commun. 46 (2007) 4949–4951.
[7] S. Nishimoto, H. Sekine, X. Zhang, Z. Liu, K. Nakata, T. Murakami, Y. Koide, A. Fujishima, Langmuir 25 (2009) 7226–7228.
[8] Y.K. Lai, F. Pan, C. Xu, H. Fuchs, L.F. Chi, Adv. Mater. 25 (2013) 1682–1686.
[9] W. Guo, T.A. Brown, B.M. Fung, J. Phys. Chem. 95 (1991) 1829–1836.
[10] Y. Kuwahara, T. Kamegawa, K. Mori, H. Yamashita, Chem. Commun. 478 (2008) 3–4785.

[11] T. Shimada, K. Aoki, Y. Shinoda, T. Nakamura, N. Tokunaga, S. Inagaki, T. Hayashi, J. Am. Chem. Soc. 125 (2003) 4688–4689.
[12] M.Y. Xing, D.Y. Qi, J.L. Zhang, F. Chen, B.Z. Tian, S. Bagwas, M. Anpo, J. Catal. 294 (2012) 37–46.
[13] C. Kapridaki, L. Pinho, M.J. Mosquera, P.M. Kalaitzaki, Appl. Catal. B: Environ. 156–157 (2014) 416–427.
[14] B.C. Qiu, M.Y. Xing, J.L. Zhang, J. Am. Chem. Soc. 136 (2014) 5852–5855.
[15] M.M. Gao, C.K.N. Peh, W.L. Ong, G.W. Ho, RSC Adv. 3 (2013) 13169–13177.
[16] W.J. Han, L. Ren, L.J. Gong, X. Qi, Y.D. Liu, L.W. Yang, X.L. Wei, J.X. Zhong, ACS Sust. Chem. Eng. 2 (2014) 741–748.
[17] Z.Y. Zhang, F. Xiao, Y.L. Guo, S. Wang, Y.Q. Liu, ACS Appl. Mater. Interfaces 5 (2013) 2227–2233.
[18] H.C. Bi, X. Xie, K.B. Yin, Y.L. Zhou, S. Wan, L.B. He, F. Xu, F. Banhart, L.T. Sun, R.S. Ruoff, Adv. Funct. Mater. 22 (2012) 4421–4425.
[19] S. Nardecchia, D. Carriazo, M.L. Ferrer, M.C. Gutiérrez, F. del Monte, Chem. Soc. Rev. 42 (2013) 794–830.
[20] J. Biener, M. Stadermann, M. Suss, M.A. Worsley, M.M. Biener, K.A. Rose, T.F. Baumann, Energy Environ. Sci. 41 (2011) 656–667.
[21] Y.X. Xu, K.X. Sheng, C. Li, G.Q. Shi, ACS Nano 4 (2010) 4324–4330.
[22] W.J. Liu, Y.K. Wang, Z.H. Li, Chem. Commun. 50 (2014) 10311–10314.
[23] A. Lerf, H.Y. He, M. Forster, J. Phys. Chem. B 102 (1998) 4477–4482.
[24] J. Qiu, P. Zhang, M. Ling, S. Li, P. Liu, H. Zhao, S. Zhang, ACS Appl. Mater. Interfaces 4 (2012) 3636–3642.
[25] P. Lian, X. Zhu, S. Liang, Z. Li, W. Yang, H. Wang, Electrochim. Acta 55 (2010) 3909–3914.
[26] C.K. Chua, M. Pumera, Eur. J. Chem. 19 (2013) 2005–2011.
[27] S.M. Luzan, A.V. Talyzin, J. Phys. Chem. C 115 (2011) 24611–24614.
[28] S. Chen, J.W. Zhu, X.D. Wu, Q.F. Han, X. Wang, ACS Nano 4 (2010) 2822–2830.
[29] D.V. Bavykin, V.P. Dubovitskaya, A.V. Vorontsov, V.N. Parmon, Res. Chem. Intermed. 33 (2007) 449–464.
[30] N. Li, G. Liu, C. Zhen, F. Li, L.L. Zhang, H.M. Cheng, Adv. Funct. Mater. 21 (2011) 1717–1722.
[31] S.X. Yu, L.W. Yang, Y. Tian, P. Yang, F. Jiang, S.W. Hu, X.L. Wei, J.X. Zhong, J. Mater. Chem. A 1 (2013) 12750–12758.